RSC Advances

ROYAL SOCIETY OF CHEMISTRY

www.rsc.org/advances

Text and graphic of table of content

Using synchrotron small angle X-ray scattering (SAXS), self-assembly of ionic supramolecules based upon diblock copolymers of poly(styrene)-*b*-poly(methacrylic acid) and multi-tail (2- or 4-tail) alkyl quaternary ammonium amphiphiles is investigated.

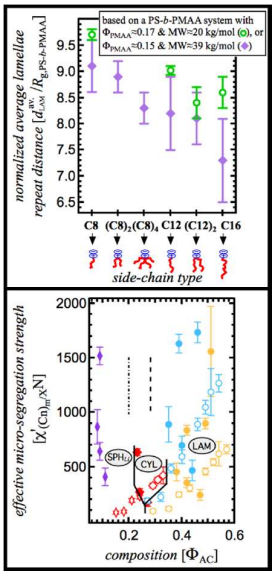

Journal Name

RSCPublishing

ARTICLE

Self-assembly of block copolymer-based ionic supramolecules based upon multi-tail amphiphiles

Cite this: DOI: 10.1039/xoxxoooooox

M. Asad Ayoubi,*[a] K. Almdal,[b] K. Zhu,[c] B. Nyström,[c] U. Olsson,[a] and L. Piculell[a]

Received ooth January 2012,
Accepted ooth January 2012

DOI: 10.1039/xoxxoooooox

www.rsc.org/

Utilising simple acid-base titration chemistry, a new family of Linear-*b*-Amphiphilic Comb (L-*b*-AC) ionic supramolecules [*Soft Matter* **2013**, *9*, 1540-1555] featuring *multi-tail* side-chains have been synthesized and examined by synchrotron SAXS. To three different parent diblock copolymers of poly(styrene)-*b*-poly(methacrylic acid) PS-*b*-PMAA multi-tail ammonium side-chains of $(C8)_2$-, $(C8)_4$- or $(C12)_2$-type were attached at various side-chain grafting densities (X), making it possible to separate effects of the details of the AC-block architecture from effects of the overall volume fraction of the AC block. The micro-segregated morphologies of these systems include AC-block filled spherical microdomains in a liquid-like state (SPH_{LL}), AC-block filled hexagonally-packed cylinders (CYL), alternating lamellar microlayers of AC- and L-blocks (LAM) and L-block filled hexagonally-packed cylinders (CYL*). For systems with the same parent diblock copolymer that also carry a constant volume fraction of AC-blocks, an increase in the side-chain length (l_{sc}) and/or in the number of alkyl tails (m) in the side-chain result in a microdomain morphology that is either unchanged or changed into one with a *less* curved interface. For lamellae-forming L-*b*-AC ionic supramolecules made up of the same parent diblock copolymer, a body of experimental data showing small variations in the repeat distance of the LAM micro-segregated structure (d_{LAM}) could be obtained by making appropriate combinations of X, l_{sc} and m. For such lamellae-forming L-*b*-AC ionic supramolecules, the average of d_{LAM} values *decreases* when l_{sc} and/or m *increase*. For systems with $(C12)_2$-type side-chains, the effective Flory-Huggins parameter between L- and AC-blocks $\chi'_{(C12)_2/X}$ was determined at various side-chain grafting densities and it was observed that $\chi'_{(C12)_2/X}$ increases when X is increased.

1. Introduction

Self-assembly of block copolymer-based systems has always been an active area of research, because of its fundamental significance and numerous useful applications.[1-3] For the melt of a linear A-*b*-B diblock copolymer, the interfacial tension between A- and B-blocks can drive the system into a micro-segregated state with segregated A- and B-rich microdomains. For a particular choice of A- and B-repeat units, when the microdomains are well segregated (i) the shape of the microdomains only depends on the volume ratio of the two blocks,[4, 5] and (ii) for a particular microdomain shape, at a given temperature, the domain size only depends on the total number of segments of the linear A-*b*-B diblock copolymer.[6]

In fundamental and application-related studies that involve melts of block copolymers, one approach to control the system's self-assembly characteristics (e.g., the shape or the size of its segregated microdomains) is through fine-tuning the molecular characteristics of the used macromolecules, e.g., their structural, compositional, and chemical properties. One method to achieve this goal is through application of principles of supramolecular chemistry that allows attachment of low-molecular-weight amphiphiles to one of the blocks of a linear A-*b*-B diblock copolymer through physical bonds, e.g., *via* hydrogen[7-10] or ionic[11-13] bonds. In this way, a parent linear A-*b*-B macromolecule is transformed into a supramolecule that consists of one linear block (A-block) and one comb-like block (made up of a parent B-block and amphiphile molecules), i.e., a linear-*b*-comb-like supramolecule. Thus, for example, by simply adjusting the amount of the added amphiphile one is able to conveniently control the volume fraction of the comb-like block $\Phi_{comb-like}$.

In the above-mentioned linear-*b*-comb-like supramolecules, micro-segregation (between linear and comb-like blocks) and nano-segregation (within the comb-like blocks, between their polar backbone and non-polar side-chains) can occur simultaneously, giving rise to a variety of structure-*in*-structure self-assemblies.[7-12, 14-17]

As well as being interesting from the point of view of fundamental research, such linear-*b*-comb-like supramolecules have recently attracted a lot of attention due to their possible nanotechnological applications.[18-22] For example, because

varying $\Phi_{comb-like}$ is easy for such materials, controlling the shape and the size of the microdomains appears to be a straightforward task – in analogy with the physics of a well-segregated linear A-*b*-B diblock copolymer system. On the other hand, because of the topology, a large volume fraction of the comb-like block resides in its side-chains (i.e., the attached amphiphiles). This means that, in the micro-segregated state, the backbone of the comb-like block must adopt a (highly) stretched conformation to fill the middle of the comb-like domains uniformly.[23] In order to avoid this large loss of conformational entropy, the system might be micro-segregated into a microdomain morphology that is different from that of a well-segregated conventional linear A-*b*-B diblock copolymer system.[24] For example, in n-miktoarm star copolymers[25-27] (i.e., when one linear A-block and n-1 linear B-blocks are joint together at one end), or a copolymer composed of one linear A-block and one comb B-block,[28] for nearly compositionally symmetric systems (i.e., $\Phi_A \cong 0.5$), instead of a lamellar structure, the system is micro-segregated into a cylindrical microdomain morphology, where the A-blocks are found in the discrete domains and the B-blocks are in the matrix. Thus, an interesting question will be how, in a linear-*b*-comb-like supramolecule, the shape and the size characteristics of the microdomains change when the topology of the comb-like block is changed at a fixed $\Phi_{comb-like}$. More specifically, it is desirable to know how *changing the topology of the attached amphiphiles* – e.g., by varying the number of 'tails' that are joint to the amphiphile head-group – affects the shape and the size characteristics of the microdomains of the resultant block copolymer-based supramolecule. To our knowledge, this has not previously been systematically studied.

In refs.[12, 23] we presented results for a new class of block copolymer-based ionic supramolecules based on parent diblock copolymers of poly(styrene)-*b*-poly(methacrylic acid) PS-*b*-PMAA. Each supramolecule contained one linear block (L-block) and one *strongly* amphiphilic comb-like block (AC-block), making up a L-*b*-AC ionic supramolecule. In our previous studies,[12, 23] the AC blocks of the L-*b*-AC ionic supramolecules were comb-like copolymers in which single-tail alkyl side-chains were ionically attached to the linear backbone of poly(methacrylate) PMA (see Schemes 1 and 2 of ref.[12] or Figure 1 of ref.[23]). Regarding the *shape* and the *size* characteristics of micro-segregated state of single-tail containing L-*b*-AC ionic supramolecules, the key results of the afore-mentioned two studies are the following. (*1*) The shape of the microdomains only depends on Φ_{AC}, regardless of the composition and the molecular weight of the parent diblock copolymer, or the length (l_{sc}) or grafting density (X) of the alkyl side-chains.[12] (*2*) Analysis of the lamellar microdomains showed that when there is an increase in X, l_{sc} or both, there is an increase in *both* the average interfacial area per block junction Σ_{LAM} and the thickness of the microlayer of the AC-block, d_{AC}.[23]

Thus, having established the relationships between the molecular properties of *single*-tail containing L-*b*-AC ionic supramolecules and the shape and the size characteristics of (lamellar) microdomains, the main aim of the present paper is to explore in detail the relationship between such properties and the shape and the size characteristics of *multi*-tail containing L-*b*-AC ionic supramolecules. The multi-tail alkyl side-chains are based on the cationic quaternary ammonium surfactants dioctyldimethylammonium [$(C8)_2$-type], didodecyldimethylammonium [$(C12)_2$-type], and tetraoctylammonium [$(C8)_4$-type]. Topologically, the resultant L-*b*-AC systems are novel and unique, because, owing to the specific chemistry of quaternary ammonium surfactants, all alkyl tails of a multi-tail side-chain emanate from a single atom (i.e., a 'point'). Thus, the experimental results of the present study are helpful to test theoretical models, because, in certain theoretical approaches,[29, 30] the comb-like block of a model block copolymer consists of a number of branch points, from each of which several side-chains emanate.

The studied systems of the present paper are based on three different parent PS-*b*-PMAA diblock copolymers (S-MAA-M-17, S-MAA-15 and S-MAA-8-M; see Table 1 for their molecular and structural characteristics) and multi-tail alkyl side-chains of $(C8)_2$-, $(C8)_4$- or $(C12)_2$-type at various side-chain grafting densities X (X=number of multi-tail alkyl side-chains per acidic group of the parent PMAA block) [see Scheme 1]. [Such systems are symbolized as name of the parent diblock copolymer/$(Cn)_m$/X, e.g., S-MAA-15/$(C8)_4$/0.9].

2. Experimental

Our block copolymer-based ionic supramolecules are prepared by an acid-base reaction between the acidic groups of the PMAA blocks of PS-*b*-PMAA diblock copolymers and the hydroxide forms of the various quaternary ammonium surfactants at various side-chain grafting densities. In this process water is eliminated and the multi-chain alkyl side-chains [$(Cn)_m$, n/m=12/2, 8/2, and 8/4] are tightly attached to the parent PMAA backbone through the (dimethyl)ammonium carboxylate ion pairs (see Scheme 1).

2.1. Materials

S-MAA-15 was purchased from Polymer Source. S-MAA-17-M and S-MAA-8-M were synthesized through the method of atom transfer radical polymerization (ATRP). Details of synthesis and characterization can be found in ref.[31]

The surfactants didodecyldimethylammonium bromide [$(C12)_2$DABr] and tetraoctylammonium bromide [$(C8)_4$ABr] were obtained from Sigma Aldrich and dioctyldimethylammonium bromide [$(C8)_2$DABr] was purchased from TCI Europe. The DOWEX MONOSPHERE 550 A (OH) anion exchange resin was obtained from Sigma Aldrich.

2.2. Sample Preparation

The surfactants were converted to their hydroxide forms [$(C12)_2$DAOH, $(C8)_4$AOH and $(C8)_2$DAOH] by an ion-exchange reaction as described before[32] and the dried $(C12)_2$DAOH, $(C8)_4$AOH and $(C8)_2$DAOH powders were

obtained after freeze-drying for several days.[12] Our samples of L-*b*-AC ionic supramolecules were prepared by adding desired small aliquots of $(C12)_2$DAOH, $(C8)_4$AOH or $(C8)_2$DAOH as concentrated water/THF solutions to appropriate amounts of dioxane solutions of parent PS-*b*-PMAA diblock copolymers followed by solvent evaporation and annealing steps, as was described in detail elsewhere.[12]

2.3. SAXS Measurements

SAXS measurements were performed at beamline I911-4 at the MaxLab synchrotron facility in Lund, Sweden. The intensity I(q) was measured at room temperature as a function of the scattering vector q [$q = (4\pi/\lambda)\sin\theta$, where 2θ is the scattering angle and the wavelength of the X-ray beam was λ = 0.91 (Å)].

3. Results and Structural/Molecular Analysis

This section of the paper is divided into three parts. First, in subsection 3.1, SAXS data and the related microdomain morphology type identification of the synthesized L-*b*-AC ionic supramolecules are presented. Second, in subsection 3.2, the size characteristics of their microdomains are analyzed. Third, in subsection 3.3, the effective Flory-Huggins interaction parameter between L- and AC-blocks $\chi'_{(C12)_2/X}$ is determined for systems with $(C12)_2$-type counter-ions (i.e., side-chains), at various ion (pair) fractions X.,

3.1. SAXS Data and Microdomain Morphology Type Identification

In this subsection, SAXS data together with the details of microdomain morphology identification are presented for L-*b*-AC ionic supramolecules based on the parent diblock copolymers of S-MAA-15 (in subsection 3.1.1), S-MAA-17-M (in subsection 3.1.2), and S-MAA-8-M (in subsection 3.1.3).

3.1.1. Systems Based on Compositionally Asymmetric S-MAA-15

The results of SAXS experiments are presented for L-*b*-AC ionic supramolecules that are based on the compositionally asymmetric parent diblock copolymer of S-MAA-15 and side-chains of the type $(C12)_2$ (see Figure 1, a and d), $(C8)_2$ (see Figure 1, b and e), and $(C8)_4$ (see Figure 2) with various side-chain grafting densities X ($0.1 \leq X \leq 1.0$).

For systems based on $(C12)_2$ and $(C8)_2$ side-chains the identified microdomain morphologies are (AC-block)-filled hexagonally-packed cylindrical CYL [i.e., *normal* cylindrical microdomain morphology, meaning that the discrete (cylindrical) domains are filled by AC-blocks] and alternating lamellar microlayers of L- and AC-blocks LAM. In Figure 3, the microdomain morphology diagrams of these two series of samples – together with those of other series of samples – are shown as a function of the volume fraction of the AC-blocks Φ_{AC}[†] For three $(C8)_2$-based samples with X-values of 0.8, 0.9 and 1.0 the exact nature of the microdomain morphologies are not identified, but we believe the micro-segregated domains should have an anisotropic shape (e.g., lamellar), because the samples are birefringent when viewed between crossed polarizers.

For systems based on $(C8)_4$ side-chains, depending on the value of X, the details of the scattering patterns are different, as explained below. The scattering patterns of systems with an X-value in the range of $0.1 \leq X \leq 0.5$ exhibit Bragg reflections at integer relative positions, which are attributed to the micro-segregated LAM structure (see Figure 2, a) [the q-range of the first-order peak Δq_{100} and that of the second-order peak Δq_{200} are marked on the graph]. On the other hand, for systems with an X-value in the range of $0.6 \leq X \leq 1.0$, through inspection of the scattering patterns (see Figure 2, b), and comparisons of these intensity patterns with those of systems with an X-value in the range of $0.1 \leq X \leq 0.5$ (see Figure 2, a), the following observations are made. (i) In addition to the Bragg reflections, there are some intensity oscillations. (ii) While at Δq_{100} some (possible) peaks are found, no peak is observed at Δq_{200}. (iii) Bragg reflections are identified in a q-range of $0.0192\ (\text{Å}^{-1}) \leq q \leq 0.0227\ (\text{Å}^{-1})$; The position of the peak monotonically shifts to a higher q-value when X is increased. Such reflections are absent in the scattering patterns of systems with an X-value in the range of $0.1 \leq X \leq 0.5$. These observations led us to the conclusion that the microdomain morphologies of samples with an X-value in the range of $0.6 \leq X \leq 1.0$ are different from those of the samples with an X-value in the range of $0.1 \leq X \leq 0.5$, i.e., they are non-LAM. The fact that these samples – like those with an X-value in the range of $0.1 \leq X \leq 0.5$ – are birefringent when viewed between crossed polarizers indicates that their microdomains have an anisotropic shape, e.g., cylindrical.

In Figure 2, b, for the system of S-MAA-15/$(C8)_4$/1.0 two peaks are identified at $q_1 \cong 0.0131\ (\text{Å}^{-1})$ and $q_2 \cong 0.0227\ (\text{Å}^{-1})$ [$\cong \sqrt{3}\, q_1$]. Thus, we assign the microdomain morphology of the system to be L-block filled hexagonally-packed cylindrical CYL* [i.e., *reversed* cylindrical microdomain morphology, meaning that the discrete (cylindrical) domains are filled by L-blocks].

In Figure 2, b, for the system of S-MAA-15/$(C8)_4$/0.9 one peak is identified at $q_1 \cong 0.0217\ (\text{Å}^{-1})$. Also, it appears that there is another peak at $q_2 \cong 0.0125\ (\text{Å}^{-1}) \cong q_1/\sqrt{3}$. Thus, we assign the microdomain morphology of the sample to be CYL*.

In the investigated q-range, one peak for the system of S-MAA-15/$(C8)_4$/0.8 [at $q_1 \cong 0.0201\ (\text{Å}^{-1})$] and one peak for the system of S-MAA-15/$(C8)_4$/0.7 [at $q_1 \cong 0.0192\ (\text{Å}^{-1})$] are identified (see Figure 2, b). We assign these peaks as $\sqrt{3}$ reflections of the 2-D hexagonal lattices. Thus, for these two samples, the microdomain morphology is identified to be CYL*.

As mentioned above, SAXS patterns of samples with X-values in the range of $0.6 \leq X \leq 1.0$ exhibit some intensity oscillations. Such intensity oscillations in the SAXS patterns of melts of block copolymer-based systems can be caused by (i) form-factor (i.e., intra-particle) scattering of segregated microdomains with, e.g., a spherical[33] or a cylindrical[14, 31] shape, (ii) combined form-factor and inter-particle scattering[31, 34] (the latter arising from a liquid-like state of microdomains),

(iii) combined form-factor and lattice scattering,[35, 36] (iv) scattering of paracrystals exhibiting cubic symmetries,[37, 38] a 2-D hexagonally-packed cylindrical[39] or a lamellar[40] structure, or (v) overlapping of some lattice reflections[41] that could be caused by SAXS instrument smearing, lattice imperfections, etc.[42]. A detailed analysis aimed at an exact identification of the nature of the intensity oscillations of our samples is beyond the scope of the present paper, but we suggest that effects arising from form-factor scattering, lattice scattering, or both, are likely to be responsible for the appearance of such oscillations in the SAXS patterns. In the following paragraph, we provide support for this suggestion through *separate* examinations of the form-factor and the lattice scatterings.

For samples of S-MAA-15/$(C8)_4$/X, with X=0.7 (Figure 2, c), X=0.8 (Figure 2, d), and X=0.9 (Figure 2, e), the simulated intensity of the form-factor of a cylinder $P(q)$ with a radius of R and a length/radius ratio of L/R is compared with the experimental scattering pattern. For each sample the value of R, for which the simulated intensity of $P(q)$ is provided, equals the value of the radius of segregated (L-block)-filled cylindrical domains R_L obtained from volume-filling calculations, i.e., $R=R_L$. For details of the simulations we refer to the Supplementary Information. As can be seen, for each sample, (i) the simulated intensity of $P(q)$ exhibits a minimum whenever the rate of the q-dependent intensity decay of the experimental SAXS pattern experiences a sudden decrease, and (ii) the decay rate of the maxima of the simulated intensity of $P(q)$ matches well with the overall decay rate of the experimental SAXS pattern. Also, in the q-ranges at which our experimental scattering patterns show intensity oscillations, the 2-D hexagonal lattice has many closely spaced allowed reflections [e.g., see Figure 2, e, for the allowed reflections of the hexagonal structure of the system of S-MAA-15/$(C8)_4$/0.9]. It is reasonable to expect that once a few of these reflections overlap, the resultant intensity pattern rather than exhibiting a Bragg reflection may show an intensity oscillation.

3.1.2. Systems Based on Compositionally Asymmetric S-MAA-17-M

The results of SAXS experiments are presented for L-*b*-AC ionic supramolecules that are based on the compositionally asymmetric parent diblock copolymer of S-MAA-17-M and side-chains of the $(C12)_2$-type with various side-chain grafting densities X ($0.1 \leq X \leq 1.0$) [see Figure 1, c and f]. All samples are birefringent when viewed between crossed polarizers indicative of the anisotropic nature of the micro-segregated domains. The identified microdomain morphologies are CYL and LAM.

3.1.3. Systems Based on Compositionally Highly Asymmetric S-MAA-8-M

The results of SAXS experiments are presented for L-*b*-AC ionic supramolecules that are based on the compositionally *highly* asymmetric parent diblock copolymer of S-MAA-8-M and side-chains of the $(C12)_2$-type with various side-chain grafting densities X ($0.1 \leq X \leq 1.0$) [see Figure 4].

For systems with an X-value in the range of $0.6 \leq X \leq 0.9$, the reflections of the 2-D hexagonal lattice can be identified (see Figure 4, f-i). Thus, we assign the microdomain morphology of these samples to be CYL.

The following observations are made when the SAXS patterns of systems with an X-value in the range of $0.1 \leq X \leq 0.5$ (Figure 4, a-e) are compared with those of systems with an X-value in the range of $0.6 \leq X \leq 0.9$ (Figure 4, f-i). (i) Upon an increase in X, while the position of the first SAXS peak (q^*) of systems with an X-value in the range of $0.1 \leq X \leq 0.5$ shifts to a *lower* q-value, that of systems with an X-value in the range of $0.6 \leq X \leq 0.9$ shifts to a *higher* q-value (see Figure 5). (ii) The SAXS patterns of systems with an X-value in the range of $0.1 \leq X \leq 0.5$ lack peaks that can be identified as higher order Bragg reflections – as mentioned above, such reflections are present in the SAXS patterns of systems with an X-value in the range of $0.6 \leq X \leq 0.9$. (iii) The SAXS patterns of systems with an X-value in the range of $0.1 \leq X \leq 0.4$ exhibit (*a*) a broad intensity maximum in the q-range of $q \sim 0.06 - 0.1$ ($Å^{-1}$), and (*b*) a shoulder at *ca.* $q = 0.045$ ($Å^{-1}$). Such broad intensity maximums and shoulders are absent in the SAXS patterns of systems with an X-value in the range of $0.6 \leq X \leq 0.9$. The observations reported in (i)-(iii) led us to the conclusion that the microdomain morphologies of samples for which $0.1 \leq X \leq 0.5$ are different from those of the samples for which $0.6 \leq X \leq 0.9$, i.e., they are non-CYL. The fact that the former samples are non-birefringent when viewed between crossed polarizers suggests that their microdomains have an isotropic shape, i.e., spherical.

Following our previous work,[12] the experimental SAXS patterns of samples with an X-value in the range of $0.1 \leq X \leq 0.5$ are compared with the simulated intensity of a model system of polydisperse spheres that are interacting with a hard-sphere potential (see Figure 4, a-e; for the details of the simulation, we refer to the Supplementary Information). Very good agreement is observed between the experimental and the simulated SAXS patterns and the values of the mean radii of (AC-block)-filled spherical microdomains R'_{AC} are extracted. R'_{AC} varies in the range $68\ (Å) \leq R'_{AC} \leq 80\ (Å)$; see Table SI-1 of the Supplementary Information or Figure 6, a of the paper. Thus, we assign the micro-segregated morphology of these samples to be (AC-block)-filled spherical microdomains in liquid-like state SPH_{LL}.

Before finishing subsection 3.1, it should be mentioned that the SAXS patterns of systems containing $(C12)_2$ and $(C8)_2$ side-chains ($X \geq 0.3$) exhibit broad peaks centered at q values of $\cong 0.22$ ($Å^{-1}$) and $\cong 0.32$ ($Å^{-1}$), respectively (see Figure SI-1 of the Supplementary Information). These q-values are almost the same as the q-values at which systems with single-tail side-chains of the same length (l_{sc}) exhibit their nano-segregation related broad peaks.[23] Thus, we propose that the above-mentioned systems of the present study are nano-segregated. Additionally, we point out that for the samples with $(C8)_4$ side-chains, although for some of them an intensity increase can be observed at the intermediate q-range, the data of the investigated q-range is not conclusive about the occurrence of nano-segregation [see Figure SI-1 of the Supplementary Information]. Thus, based on the available SAXS data, we

cannot confirm the occurrence of nano-segregation for samples with $(C8)_4$ side-chains.

3.2. Size Characteristics of Microdomains

In this subsection we have provided an analysis of size characteristics of systems exhibiting LAM (in subsection 3.2.1), and CYL or CYL* (in subsection 3.2.2) microdomain morphologies.

3.2.1. LAM Microdomain Morphology

In our previous study[23] of lamellae-forming L-*b*-AC ionic supramolecules based on single-tail side-chains, we showed that there are correlations between a molecular characteristic of the system, namely the average molecular cross-sectional area of the AC-block σ, and two self-assembly characteristic of the system, namely the average interfacial area per block junction Σ_{LAM} and the thickness of the microlayer of the AC-block d_{AC}. [The AC-block cross-sectional area is obtained as $\sigma = V_{AC}/(Z_{PMAA}\lambda_{con})$, where V_{AC} is the molecular volume of an AC-block[†] and λ_{con} (= 2.5 Å) is the contour length of the repeat unit of the parent PMAA block.] More specifically, there is an increase in Σ_{LAM} and d_{AC} when σ is increased. Thus, for lamellae-forming L-*b*-AC ionic supramolecules of the present study, it would be useful to examine variations of Σ_{LAM} and d_{AC} when σ is changed. The results are shown in Figure 7, a. It is observed that, for systems based on the same parent diblock copolymer, Σ_{LAM} increases linearly with σ.

3.2.2. CYL and CYL* Microdomain Morphologies

In Figure 7, b, using the data of two series of samples, variations of the size characteristics of microdomains of the type *normal* cylindrical (CYL) and *reversed* cylindrical (CYL) with σ are shown. Thus, we have considered the following size characteristics: (i) the 2-D hexagonal lattice parameters (d_{CYL} and $d_{\mathrm{CYL}*}$), (ii) the interfacial areas per block junction (Σ_{CYL} and Σ_{CYL*}), (iii) the radii of microdomains (R_{AC} and R_{L}), and (iv) the minimum distances between the cylindrical microdomains (δ_L and δ_{AC}). It is observed that when σ is increased (*1*) the interfacial areas per block junction increase and, consequently, R_{L} and δ_L decrease, (*2*) for the AC-block filled domains, interestingly, while R_{AC} increases, δ_{AC} remains practically unchanged, and (*3*) the 2-D hexagonal lattice parameters decrease.

3.3. Effective Flory-Huggins Interaction Parameter

Following our previous work,[23] for systems with $(C12)_2$-type side-chains at various grafting densities X, we have used the experimental data of lamellae-forming samples, and the self-consistent field theory for an A-*b*-B diblock copolymer of Helfand and Wasserman (HW),[43] to determine the effective Flory-Huggins interaction parameter between L- and AC-blocks $\chi'_{(C12)_2/X}$ (see Figure 8). In brief, for an ion (pair) fraction of X, $\chi'_{(C12)_2/X}$ is determined using values of d_{LAM} of two lamellae-forming samples – one based on S-MAA-15 and another on S-MAA-17-M – by application of linear regression procedure to the derived equation[43-45] of $d_{LAM}^7 = K\chi'_{(C12)_2/X}$. Here K is a function of the molecular characteristics of the L- and AC-blocks and can be estimated for a L-*b*-AC ionic supramolecule; details of the calculations can be found elsewhere[23]..

4. Discussion

This section is divided into two parts. First, in subsection 4.1, the microdomain morphology of L-*b*-AC ionic supramolecules is discussed. Second, in subsection 4.2, the effective Flory-Huggins interaction parameter between L- and AC-blocks for systems neutralized by $(C12)_2$-type counter-ions (i.e., side-chains) at various side-chain grafting densities X, $\chi'_{(C12)_2/X}$, is examined.

4.1. Microdomain Morphology

4.1.1. General Remarks

The micro-segregated morphologies of multi-tail side-chain containing L-*b*-AC ionic supramolecules of the present study include AC-block filled spherical microdomains in liquid-like state SPH_{LL}, AC-block filled hexagonally-packed cylinders CYL, alternating lamellar microlayers of L- and AC-blocks LAM, and L-block filled hexagonally-packed cylinders CYL* (see Figure 3). The observation of the CYL* microdomain morphology for (S-MAA-15)-based systems is particularly interesting, because such a microdomain morphology was not obtained for single-tail side-chain containing L-*b*-AC systems based on the parent diblock copolymer S-MAA-17-M (which has a PMAA volume fraction similar to that of S-MAA-15; see Table 1), despite the fact that similar AC-block volume fractions were explored.[23] This feature thus seems to be a consequence of the novel multi-tail geometry of the side-chains used in the present work.

For systems that have the same parent diblock copolymer, through inspection of the microdomain morphology diagram of Figure 3, the following observations are made. (i) For systems that have the same type of side-chains, the shape of the microdomains depends on the volume fraction of the AC-block, in agreement with what was reported before for single-tail side-chain containing L-*b*-AC ionic supramolecules.[12] (ii) Keeping Φ_{AC} unchanged, when there is an increase in the side-chain length (l_{sc}), the number of alkyl chains (tails) at a side-chain branch point (m), or both l_{sc} and m, the microdomain morphology either remains unchanged or changes into one with a *less* curved interface.[§] This means that, contrary to the single-tail side-chain containing L-*b*-AC ionic supramolecules,[12] the volume fraction of the AC-block is *not* the only parameter that controls the shape of the microdomains.

4.1.2. Microdomain Morphological Changes

For L-*b*-AC ionic supramolecules of the present paper that are based on the same parent diblock copolymer and side-chain, the microdomain morphological changes of $\mathrm{SPH}_{LL} \rightarrow$ CYL [for systems of S-MAA-8-M/$(C12)_2$/X], CYL → LAM [for systems of S-MAA-15/$(C8)_2$/X] and LAM → CYL* [for systems of S-MAA-15/$(C12)_2$/X] are observed when Φ_{AC} (or, equivalently, X or the average molecular cross-sectional area of the AC-block σ) is increased (see Figures 3 and 6). We found that, upon the occurrence of these microdomain morphological

changes, to a good approximation, the trend of the increase of the value of the interfacial area per block junction with σ remains unchanged (see Figure 6). Also, interestingly, it is observed that, upon the occurrence of the microdomain morphological change of $SPH_{LL} \rightarrow CYL$, the radius of the microdomains continues to smoothly increase, without any abrupt change in its value, when σ is increased (see Figure 6, a).

4.1.3. CYL AND LAM MICRODOMAIN MORPHOLOGIES

For L-*b*-AC ionic supramolecules of S-MAA-15/$(C8)_4$/X ($0.1 \leq X \leq 1.0$), for (nearly) compositionally symmetric systems (i.e., with $\Phi_{AC} \cong 0.5$), the microdomain morphology changes from LAM to CYL* when Φ_{AC} is increased (see Figure 3). We hypothesize that the appearance of the CYL* instead of the LAM microdomain morphology is related to the comb-like architecture of the AC-block in the following manner. [The argument is similar that given in ref.[24] for a 3-miktoarm star ('Y-shaped') copolymer of one A-block and two B-blocks.] Consider a well-segregated lamellar layer of L-*b*-AC ionic supramolecules with $\Phi_{AC} \cong 0.5$. In this lamellar layer, the thicknesses of the AC-block and the L-block microlayers are equal. This means that both the L-block, and the poly(methacrylate) PMA backbone of the AC-block, are stretched to the same length. However, the estimated unperturbed radius of gyration of the L-block is more than two times larger than that of the PMA chain, indicating that the latter should adopt a significantly more stretched conformation.[¶] Therefore, the L/AC interface tends to bend, so that the AC-block is located on the outside of the curved interface. Thus, the AC-block finds some volume close to the interface without a need to stretch to such a large extent. Experimental support for this hypothesis is provided by the status of the AC-block backbone stretching as inferred from the characteristic sizes of the (AC-block)-filled domains of the observed LAM and CYL* structures – i.e., the thickness of the microlayer of the AC-block d_{AC} and the minimum distance between the L-block cylinders δ_{AC}, respectively (see Figure 6, c). As can be seen in Figure 6, c, when there is an increase in σ (or, equivalently, in X or Φ_{AC}), while an AC-block backbone of the LAM structure adopts a more stretched conformation, the extent of the AC-block backbone stretching in the CYL* structure remains unchanged. This is schematically depicted in Scheme 2. Thus, once there is an increase in σ, systems of S-MAA-15/$(C8)_4$/X ($0.7 \leq X \leq 1.0$), by micro-segregating into a CYL* rather than a LAM structure, do not experience a further loss in the conformational entropy of their AC-block PMA backbone.

In hydrogen-bonded stoichiometric Linear-*b*-Comb supramolecules based on poly(styrene)-*b*-poly(4-vinylpyridine) diblock copolymers and 3-*n*-pentadecyl phenol,[8] the lowest composition at which the CYL* microdomain morphology can be found is $\Phi_{Comb} \cong 0.57$. Similarly, for n-miktoarm star copolymers[25-27] (i.e., when one linear A-block and n-1 linear B-blocks are joint together at one end), and for a copolymer composed of one linear A-block and one comb B-block,[28] the nearly compositionally symmetric systems ($\Phi_A \cong 0.5$) are micro-segregated into a cylindrical microdomain morphology, where the A-blocks are found in the discrete domains and the B-blocks are in the matrix. We should also add that, from the point of view of the existence of a high thermodynamic incompatibility between L- and AC-blocks (which is due to the non-polar nature of the L-block and the polar ionic nature of the AC-block), the occurrence of CYL* microdomain morphology for our (nearly) compositionally symmetric samples is in line with the experimental observation of non-lamellar morphologies for melts of (nearly) compositionally symmetric systems of neutral-*b*-charged diblock copolymers.[46-48]

4.1.4. CYL VS. LAM MICRODOMAIN MORPHOLOGY

For systems of S-MAA-8-M/$(C1)_2$/X ($0.6 \leq X \leq 0.9$), as implicitly pointed out before,[§] there is this anomalous observation that they exhibit CYL microdomain morphology at a Φ_{AC} range where the LAM microdomain morphology is expected to occur for both single-tail (see Figure 9) and multi-tail (see Figures 4 and 11) side-chain containing L-*b*-AC ionic supramolecules. For these L-*b*-AC ionic supramolecules, based on the *highly* asymmetric parent diblock copolymer S-MAA-8-M ($\Phi_{PMAA} = 0.08$; see Table 1), we propose that the physics behind adoption of CYL instead of LAM microdomain morphology is related to the simultaneous presence of two molecular (architectural) properties, namely (i) a high degree of micro-segregation between L and AC blocks $\chi'_{(C12)_2/X}N$ [$= 376 \pm 47$; N is the total number of segments of a L-*b*-AC ionic supramolecule calculated using a reference segmental volume of v_0=100 (Å^3)], and (ii) the comb-like architecture of AC-blocks with bulky side-chains (inside the AC-blocks, the estimated volume fraction of the PMA part of the backbones ϕ_{PMA} is low; $\phi_{PMA} = 0.18 \pm 0.02$), as explained in the following. For these systems and because of high $\chi'_{(C12)_2/X}N$ values, the PMA backbones of the AC-blocks are forced to adopt a *highly* stretched conformation in the micro-segregated state, so that the amount of the interfacial contact between L- and AC-blocks is adequately reduced. Using the HW theory[43] and the obtained values of $\chi'_{(C12)_2/X}$ (see subsection 3.3 and Figure 8) for the hypothetical alternative LAM microdomain morphology for these samples, the estimated half-thickness of the microlayer of the AC-blocks is calculated to be 39±2 (Å), which is close to the contour length of the PMA backbone of the AC-block λ [$\lambda = 45$ (Å)]). Thus, if the system were micro-segregated into LAM microdomain morphology, *all* the AC-blocks should adopt a nearly fully stretched conformation, to make their domains uniformly filled. On the other hand, when the system is micro-segregated into CYL microdomain morphology, on moving from the L/AC interface in the perpendicular direction toward the center of the cylindrical microdomains the volume filled by the chains drops by a rate of (microdomain radius)$^{-1}$. Therefore, the presence of only *a few* highly stretched AC-blocks ensures that the cylindrical microdomains are uniformly filled. Thus, the anomalous observation, that systems of S-MAA-8-M/$(C1)_2$/X ($0.6 \leq X \leq 0.9$) exhibit CYL microdomain morphology at a Φ_{AC} range where the LAM microdomain morphology is expected to occur, is explained.

4.1.5. LAM MICRODOMAIN MORPHOLOGY

For lamellae-forming L-*b*-AC ionic supramolecules that are made up of the same parent diblock copolymer and side-chains – identical to the results of our previous study[23] – the following two observations are made. (i) When σ is increased the PMA part of the backbone of the AC-block adopts a more stretched conformation (i.e., d_{AC} increases; see Figure 7, a), which can be attributed to[23] (*a*) an increase in the effective degree of micro-segregation between L- and AC-blocks $\chi'_{(Cn)m/X}N$ [for the case of $(C12)_2$-containing samples, variation of d_{AC} with $\chi'_{(C12)_2/X}N$ is shown in Figure 10], and (*b*) the crowding of the atoms of the side-chains and the ion pairs in the space close to the PMA part of the backbone of the AC-block. An increase in the effective degree of nano-segregation between polar and non-polar components of the AC-block can also, contribute to this effect.[23] (ii) The average interfacial area per block junction Σ_{LAM} linearly increases with an increase in σ (see Figure 7, a).

The observation that for lamellae-forming L-*b*-AC ionic supramolecules made up of the same parent diblock copolymer and side-chains, Σ_{LAM} linearly increases when σ is increased, is the result of the fact that for such systems the variation of the repeat distance of the LAM structure d_{LAM} is small, because we have

$$\Sigma_{LAM} = (2d_{LAM}^{-1}Z_{PMAA}\lambda_{con})\sigma + 2d_{LAM}^{-1}V_L = A\sigma + B$$

, where A and B are the slope and the intercept of the equation of a line, respectively. Thus, for such systems, it would be useful to see how the parameter d_{LAM}^{av}/R_g(d_{LAM}^{av} is the average of d_{LAM} values; R_{g} is the estimated radius of gyration of the parent diblock copolymer in its unperturbed form[‡]) varies. The results are shown in Figure 11. The following observations are made. (i) For L-*b*-AC ionic supramolecules based upon the two parent diblock copolymers S-MAA-15 and S-MAA-17-M (which have similar compositions, but differ in their total degree of polymerization by a factor of two; see Table 1) values of d_{LAM}^{av}/R_g are comparable. For systems with the same side-chains, the system based on a diblock copolymer with a higher total degree of polymerization (i.e., S-MAA-15) has a smaller value of d_{LAM}^{av}/R_g. (ii) For L-*b*-AC ionic supramolecules that are based upon the same parent diblock copolymer, value of d_{LAM}^{av}/R_g *decreases*, when the side-chain length (l_{sc}), the number of alkyl chains (tails) at a side-chain branch point (*m*), or both l_{sc} and *m*, *increase*.

4.1. Effective Flory-Huggins Interaction Parameter

Variations of $\chi'_{(C12)_2/X}$ with X is presented in Figure 8. It is observed that $\chi'_{(C12)_2/X}$ increases, when X is increased.[23] Notice that, in the present work, the X-range in which the effective Flory-Huggins interaction parameter between L- and AC-blocks is determined is larger than that in ref.[23], i.e., $0.2 \leq X \leq 1.0$ *vs.* $0.8 \leq X \leq 1.0$. Additionally, for the same value of X, the value of $\chi'_{(C12)_2/X}$ is comparable to the values of the effective Flory-Huggins interaction parameter between L- and AC-blocks of L-*b*-AC ionic supramolecules neutralized by single-tail alkyl-type counter-ions.[23] Also, it should be pointed out that the reported values of $\chi'_{(C12)_2/X}$ (obtained using the experimental data of lamellae-forming samples; see subsection 3.3) are internally consistent, because – utilizing results of a strong segregation regime SSR theory[49] and a self-consistent field theory study[50] for A-*b*-B diblock copolymers – when these values are used for the prediction of the domain size of systems with microdomain morphologies of SPH_{LL} [systems of S-MAA-8-M/$(C12)_2$/X ($0.2 \leq X \leq 0.5$)] and CYL [systems of S-MAA-8-M/$(C12)_2$/X ($0.7 \leq X \leq 0.9$)], (i) for SPH_{LL} microdomain morphology, for each system, the calculated theoretical radius of microdomains[49] is mostly within the system's 'mean experimental radius of microdomains ± one standard deviation', and (ii) for CYL microdomain morphology, the calculated theoretical radii of microdomains[50] are within (5±3)% of the experimental ones.

5. Conclusions

L-*b*-AC ionic supramolecules have been synthesized using three different parent diblock copolymers of PS-*b*-PMAA and *multi-tail* alkyl side-chains of $(C8)_2$-, $(C8)_4$- and $(C12)_2$-type at various side-chain grafting densities X. The multi-tail side-chains offer a new, previously unexplored, route to change the composition and architecture of the AC block. It was found that these systems micro-segregate into SPH_{LL}, CYL, LAM and CYL* microdomain morphologies. Also, it was observed that, for systems that have the same parent diblock copolymer, keeping Φ_{AC} unchanged, when there is an increase in the side-chain length (l_{sc}), the number of alkyl chains (tails) at a side-chain branch point (*m*), or both l_{sc} and *m*, the microdomain morphology either remains unchanged or changes into one with a *less* curved interface. This is different from the previous results for analogous L-*b*-AC ionic supramolecules with *single-tail* side-chains, where the microdomain morphology only depended on Φ_{AC}. Additionally, for lamellae-forming L-*b*-AC ionic supramolecules, through analysis of a large amount of experimental data of the present study, as well as those obtained in our previous studies,[12, 23] it was concluded that the average repeat distance of the LAM micro-segregated structure *decreases* when l_{sc}, *m*, or both, *increase*. Finally, for systems neutralized by $(C12)_2$-type counter-ions, the determined effective Flory-Huggins parameter between L- and AC-blocks increases when the ion (pair) fraction (X) is increased.

Thus, in this paper, for a new class of hierarchically self-assembled (block copolymer+amphiphile)-based ionic supramolecules[12, 23] (i.e., L-*b*-AC ionic supramolecules), through a detailed comprehensive analysis of data of (multi-tail)-amphiphile-based systems – as well as those of (single-tail)-amphiphile-based systems of our previous studies[12, 23] – we have demonstrated how the microdomain morphology properties (including the shape and the size characteristics) can be easily fine-tuned through varying the choice of the neutralizing amphiphile counter-ion [i.e., changing its physicochemical and architectural (topological) properties] and the neutralization degree of the parent diblock copolymer. We believe the insight gained through the results of the present study could be useful in further development of both the theory

and the (potential) applications of block copolymer-based (ionic) supramolecules.

Acknowledgement

Financial support by the Swedish Research Council (VR) through the Linnaeus grant for the Organizing Molecular Matter (OMM) Center of Excellence (239-2009-6794) is gratefully acknowledged.

Notes and references

[a] Division of Physical Chemistry, Center for Chemistry and Chemical Engineering, Lund University, SE-22 100 Lund, Sweden.
[b] Department of Micro- and nanotechnology, Technical University of Denmark, DTU Nanotech, Building 423, DK-2800 Kongens Lyngby, Denmark.
[c] Department of Chemistry, University of Oslo, P.O. Box 1033, Blindern, N-0315 Oslo, Norway.

† Calculated assuming a density of 1 g cm^{-3} for poly(didodecyldimethylammonium methacrylate), poly(dioctyldimethylammonium methacrylate) and poly(tetraoctylammonium methacrylate).

§ This trend was not observed when microdomain morphologies of multi-tail side-chain containing samples of S-MAA-8-M/$(C12)_2$/X (Figure 3) were compared to those of single-tail side-chain containing samples of S-MAA-8-M/(C12)/X (ref. [12]) [the possible reasons of the deviation of the afore-mentioned multi-tail side-chain containing samples from the observed trend are discussed in subsection 4.1.4].

¶ The radii of gyration of PS block R_g^{PS} and PMAA block R_g^{PMAA} are calculated using the values of the statistical segment lengths of $b_{PS} = 6.8$ (Å) [from ref. [51]] and $b_{PMAA} = 6.2$ (Å) [estimated from the radius of gyration of an unperturbed coil of PMAA[31, 52]], respectively.

‡ R_g can be estimated from the expression $\left(R_g\right)^2 = \left(R_g^{PS}\right)^2 + \left(R_g^{PMAA}\right)^2$.

Electronic Supplementary Information (ESI) available: form-factor simulation of a cylinder; SAXS modeling of SPH_{LL} microdomains; SAXS data of the nano-segregated state. See DOI: 10.1039/b000000x/

1 I. Hamley, *Developments in Block Copolymer Science and Technology*, Wiley, 2004.
2 I. Hamley, *The Physics of Block Copolymers*, Oxford University Press, 1998.
3 S. B. Darling, *Progress in Polymer Science (Oxford)*, 2007, **32**, 1152-1204.
4 F. S. Bates and G. H. Fredrickson, *Annual Review of Physical Chemistry*, 1990, **41**, 525-557.
5 F. S. Bates, M. F. Schulz, A. K. Khandpur, S. Förster, J. H. Rosedale, K. Almdal and K. Mortensen, *Faraday Discussions*, 1994, **98**, 7-18.
6 A. N. Semenov, *Sov. Phys. JETP*, 1985, **61**, 733-742.
7 J. Ruokolainen, R. Mäkinen, M. Torkkeli, T. Mäkelä, R. Serimaa, G. Ten Brinke and O. Ikkala, *Science*, 1998, **280**, 557-560.
8 J. Ruokolainen, M. Saariaho, O. Ikkala, G. Ten Brinke, E. L. Thomas, M. Torkkeli and R. Serimaa, *Macromolecules*, 1999, **32**, 1152-1158.
9 J. Ruokolainen, G. Ten Brinke and O. Ikkala, *Advanced Materials*, 1999, **11**, 777-780.
10 S. Valkama, T. Ruotsalainen, A. Nykänen, A. Laiho, H. Kosonen, G. Ten Brinke, O. Ikkala and J. Ruokolainen, *Macromolecules*, 2006, **39**, 9327-9336.
11 A. F. Thünemann and S. General, *Macromolecules*, 2001, **34**, 6978-6984.
12 M. A. Ayoubi, K. Zhu, B. Nyström, K. Almdal, U. Olsson and L. Piculell, *Soft Matter*, 2013, **9**, 1540-1555.
13 M. R. Hammond, C. Li, C. Tsitsilianis and R. Mezzenga, *Soft Matter*, 2009, **5**, 2371-2377.
14 C. S. Tsao and H. L. Chen, *Macromolecules*, 2004, **37**, 8984-8991.
15 B. Nandan, C. H. Lee, H. L. Chen and W. C. Chen, *Macromolecules*, 2005, **38**, 10117-10126.
16 B. Nandan, C. H. Lee, H. L. Chen and W. C. Chen, *Macromolecules*, 2006, **39**, 4460-4468.
17 G. G. D. Sart, I. Vukovic, G. A. Van Ekenstein, E. Polushkin, K. Loos and G. T. Brinke, *Macromolecules*, 2010, **43**, 2970-2980.
18 S. Valkama, T. Ruotsalainen, H. Kosonen, J. Ruokolainen, M. Torkkeli, R. Serimaa, G. Ten Brinke and O. Ikkala, *Macromolecules*, 2003, **36**, 3986-3991.
19 S. Bondzic, J. De Wit, E. Polushkin, A. J. Scheuten, G. T. Brinke, J. Ruokolainen, O. Ikkala, I. Dolbnya and W. Bras, *Macromolecules*, 2004, **37**, 9517-9524.
20 T. Ruotsalainen, J. Turku, P. Heikkilä, J. Ruokolainen, A. Nykänen, T. Laitinen, M. Torkkeli, R. Serimaa, G. T. Brinke, A. Harlin and O. Ikkala, *Advanced Materials*, 2005, **17**, 1048-1052.
21 T. Ruotsalainen, J. Turku, P. Hiekkataipale, U. Vainio, R. Serimaa, G. T. Brinke, A. Harlin, J. Ruokolainen and O. Ikkala, *Soft Matter*, 2007, **3**, 978-985.
22 B. Nandan, B. K. Kuila and M. Stamm, *European Polymer Journal*, 2011, **47**, 584-599.
23 M. Asad Ayoubi, K. Almdal, K. Zhu, B. Nyström, U. Olsson and L. Piculell, *Macromolecules*, 2014, **47**, 3428-3435.
24 S. T. Milner, *Macromolecules*, 1994, **27**, 2333-2335.
25 S. P. Gido and Z.-G. Wang, *Macromolecules*, 1997, **30**, 6771-6782.
26 N. Hadjichristidis, H. Iatrou, S. K. Behal, J. J. Chludzinski, M. M. Disko, R. T. Garner, K. S. Liang, D. J. Lohse and S. T. Milner, *Macromolecules*, 1993, **26**, 5812-5815.
27 D. J. Pochan, S. P. Gido, S. Pispas, J. W. Mays, A. J. Ryan, J. P. A. Fairclough, I. W. Hamley and N. J. Terrill, *Macromolecules*, 1996, **29**, 5091-5098.
28 M. B. Runge, C. E. Lipscomb, L. R. Ditzler, M. K. Mahanthappa, A. V. Tivanski and N. B. Bowden, *Macromolecules*, 2008, **41**, 7687-7694.
29 L. Wang, L. Zhang and J. Lin, *The Journal of Chemical Physics*, 2008, **129**, 114905.
30 R. J. Nap and G. ten Brinke, *Macromolecules*, 2002, **35**, 952-959.
31 M. Asad Ayoubi, K. Zhu, B. Nyström, U. Olsson, K. Almdal, A. R. Khokhlov and L. Piculell, *Journal of Polymer Science Part B: Polymer Physics*, 2013, **51**, 1657-1671.
32 A. Svensson, L. Piculell, B. Cabane and P. Ilekti, *Journal of Physical Chemistry B*, 2002, **106**, 1013-1018.
33 F. S. Bates, R. E. Cohen and C. V. Berney, *Macromolecules*, 1982, **15**, 589-592.

34 D. J. Kinning and E. L. Thomas, *Macromolecules*, 1984, **17**, 1712-1718.
35 M. Schwab and B. Stühn, *Phys. Rev. Lett.*, 1996, **76**, 924-927.
36 S. Forster, A. Timmann, M. Konrad, C. Schellbach, A. Meyer, S. S. Funari, P. Mulvaney and R. Knott, *J Phys Chem B*, 2005, **109**, 1347-1360.
37 H. Matsuoka, H. Tanaka, T. Hashimoto and N. Ise, *Physical Review B*, 1987, **36**, 1754-1765.
38 H. Matsuoka, H. Tanaka, N. Iizuka, T. Hashimoto and N. Ise, *Physical Review B*, 1990, **41**, 3854-3856.
39 T. Hashimoto, T. Kawamura, M. Harada and H. Tanaka, *Macromolecules*, 1994, **27**, 3063-3072.
40 M. Shibayama and T. Hashimoto, *Macromolecules*, 1986, **19**, 740-749.
41 N. Sakamoto, T. Hashimoto, C. D. Han, D. Kim and N. Y. Vaidya, *Macromolecules*, 1997, **30**, 1621-1632.
42 R. J. Roe, *Methods of X-Ray and Neutron Scattering in Polymer Science*, Oxford University Press, 2000.
43 E. Helfand and Z. R. Wasserman, *Macromolecules*, 1976, **9**, 879-888.
44 Y. Matsushita, K. Mori, R. Saguchi, Y. Nakao, I. Noda and M. Nagasawa, *Macromolecules*, 1990, **23**, 4313-4316.
45 E. Helfand and A. M. Sapse, *J. Chem. Phys.*, 1975, **62**, 1327-1331.
46 M. J. Park and N. P. Balsara, *Macromolecules*, 2008, **41**, 3678-3687.
47 S. Y. Kim, M. J. Park, N. P. Balsara and A. Jackson, *Macromolecules*, 2010, **43**, 8128-8135.
48 H.-C. Lee, H. Lim, W.-F. Su and C.-Y. Chao, *Journal of Polymer Science Part A: Polymer Chemistry*, 2011, **49**, 2325-2338.
49 I. A. Nyrkova, A. R. Khokhlov and M. Doi, *Macromolecules*, 1993, **26**, 3601-3610.
50 M. W. Matsen and F. S. Bates, *Journal of Polymer Science, Part B: Polymer Physics*, 1997, **35**, 945-952.
51 D. G. H. Ballard, G. D. Wignall and J. Schelten, *Eur. Polym. J.*, 1973, **9**, 965-969.
52 J. Pleštil, Y. M. Ostanevich, V. Y. Bezzabotonov, D. Hlavatá and J. Labský, *Polymer*, 1986, **27**, 839-842.
53 H. Walter, C. Harrats, P. Müller-Buschbaum, R. Jérome and M. Stamm, *Langmuir*, 1999, **15**, 1260-1267.
54 J. Mark, K. Ngai, W. Graessley, L. Mandelkern, E. Samulski, J. Koenig and G. Wignall, *Physical Properties of Polymers, 3rd Edition*, Cambridge University Press, 2004.

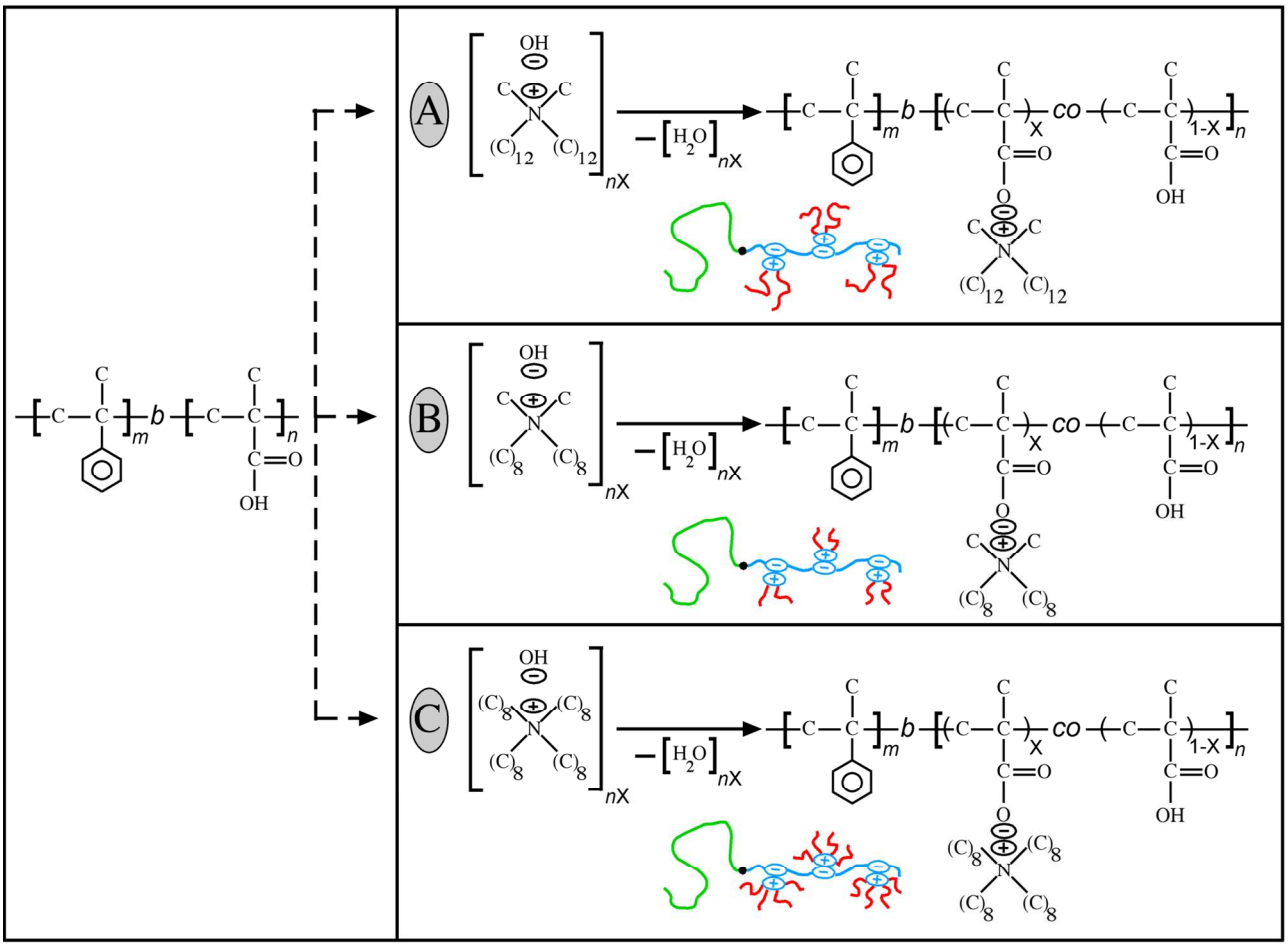

Scheme 1. Schematics of the acid-base reaction between PMAA block of a PS-*b*-PMAA diblock copolymer and (A) didodecyldimethylammonium hydroxide [$(C12)_2$DAOH], (B) dioctyldimethylammonium hydroxide [$(C8)_2$DAOH], and (C) tetraoctylammonium hydroxide [$(C8)_4$AOH] amphiphiles, and the resultant L-*b*-AC ionic supramolecule.

Table 1. Molecular and structural characteristics of the parent PS-*b*-PMAA diblock copolymers used for preparation of L-*b*-AC ionic supramolecules.

Diblock copolymer	Z_{PS} [b]	Z_{PMAA} [b]	Φ_{PMAA} [c]	Microdomain morphology [d]
S-MAA-17-M[a]	155	43	0.17	$SPH(PMAA)_{BCC}$ [e]
S-MAA-15	318	78	0.15	$SPH(PMAA)_{BCC}$ [e]
S-MAA-8-M[a]	155	18	0.08	$SPH(PMAA)_{LL}$ [f]

[a] The diblock copolymer system contains a minor fraction of architecturally symmetric triblock molecules that are composed of PS end-blocks and PMAA mid-blocks. In the ATRP synthesis, these triblock molecules are the product of a coupling reaction between two diblock macroradicals.[31]

[b] Z_i stands for the number average degree of polymerization of an i-block.

[c] Volume fraction of PMAA blocks Φ_{PMAA} is calculated from the density values ρ_{PMAA} = 1.22 g cm^{-3} (ref.[53]) and ρ_{PS} = 1.05 g cm^{-3} (ref.[54]).

[d] Determined by SAXS analysis.[31]

[e] $SPH(PMAA)_{BCC}$ stands for PMAA spherical microdomains in body-centered-cubic arrangement.

[f] $SPH(PMAA)_{LL}$ stands for PMAA spherical microdomains in liquid-like state.

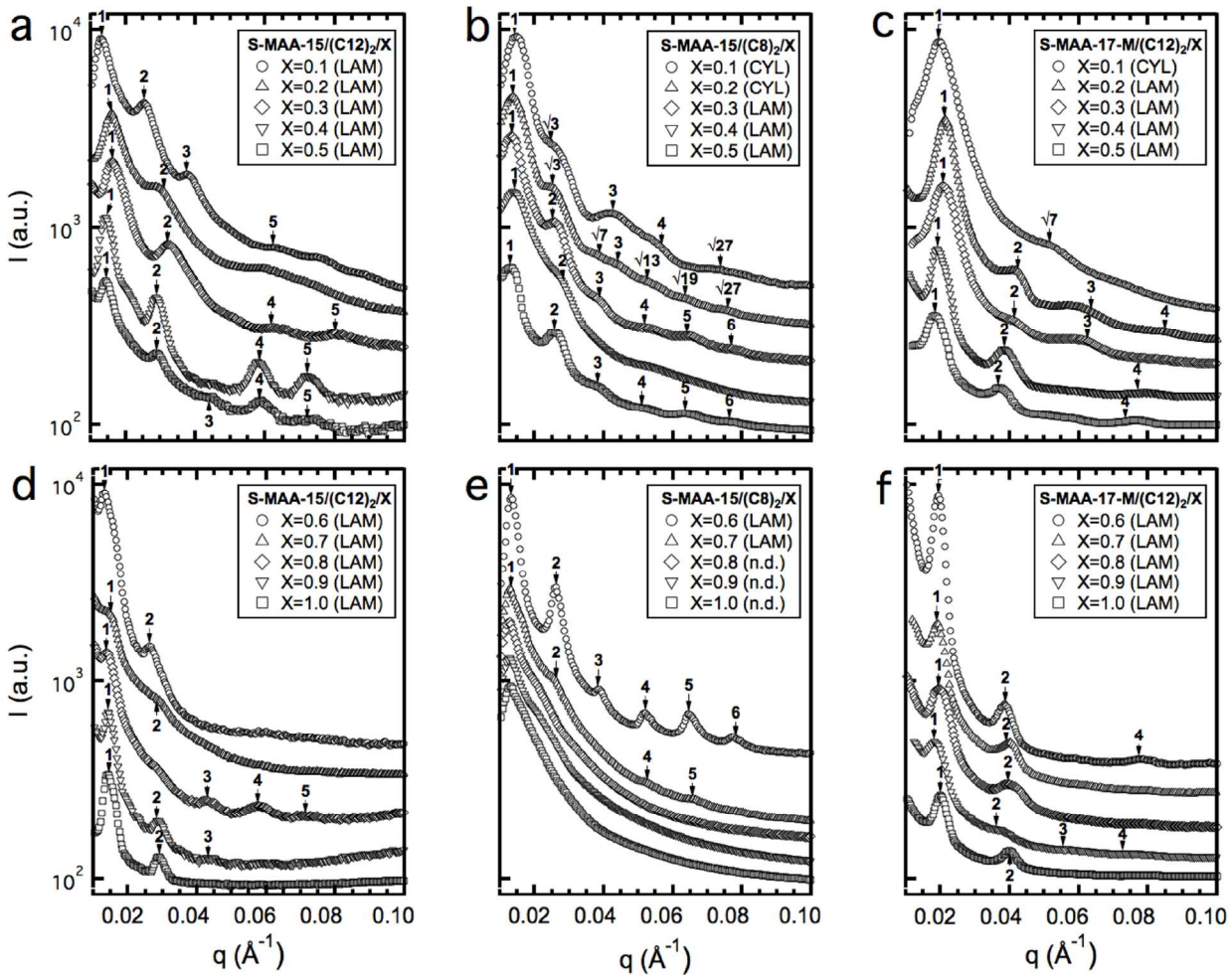

Figure 1. SAXS patterns of L-*b*-AC ionic supramolecules of [(a] and (d)] S-MAA-15/$(C12)_2$/X, [(b] and (e)] S-MAA-15/$(C8)_2$/X, and [(c) and (f)] S-MAA-17-M/$(C12)_2$/X, for [(a)-(c)] X=0.1 (circle), 0.2 (upright standing triangle), 0.3 (diamond), 0.4 (downward standing triangle) and 0.5 (square), and [(d)-(f)] X=0.6 (circle), 0.7 (upright standing triangle), 0.8 (diamond), 0.9 (downward standing triangle) and 1.0 (square). The identified microdomain morphologies of CYL and LAM and their observed reflections are indicated.

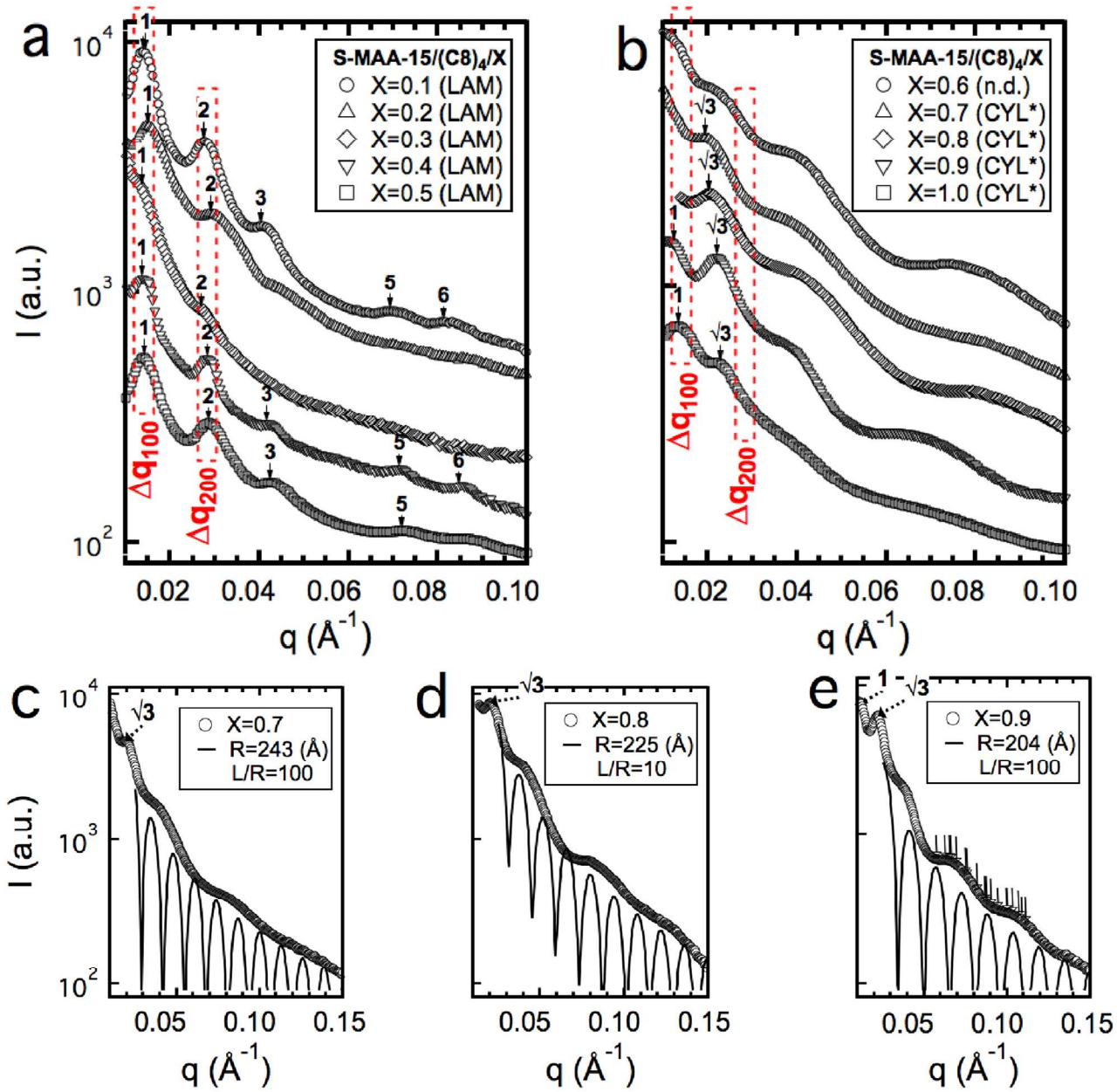

Figure 2. SAXS patterns of L-*b*-AC ionic supramolecules of S-MAA-15/$(C8)_4$/X are shown for (a) X=0.1 (circle), 0.2 (upright standing triangle), 0.3 (diamond), 0.4 (downward standing triangle) and 0.5, (b) X=0.6 (circle), 0.7 (upright standing triangle), 0.8 (diamond), 0.9 (downward standing triangle) and 1.0 (square), (c) X=0.7 (circle), (d) X=0.8 (circle), and (e) X=0.9 (circle). In (a) and (b), the identified microdomain morphologies of LAM and CYL* and their observed reflections are indicated and the q-range of the first-order peak Δq_{100} and that of the second-order peak Δq_{200} of samples with X=0.1, 0.2, 0.3, 0.4 and 0.5 are marked. In (c)-(e), the black lines are the simulated intensities of the form-factor of a cylinder $P(q)$ with a radius of R and a length/radius ratio of L/R (eqn. SI-1 of the Supplementary Information; for details of the simulation, we refer to the Supplementary Information), and the dotted lines with end-arrows are observed reflections of the CYL* microdomain morphology. In (c), the possible reflections of the CYL* microdomain morphology of the sample are shown by solid lines with end-arrows.

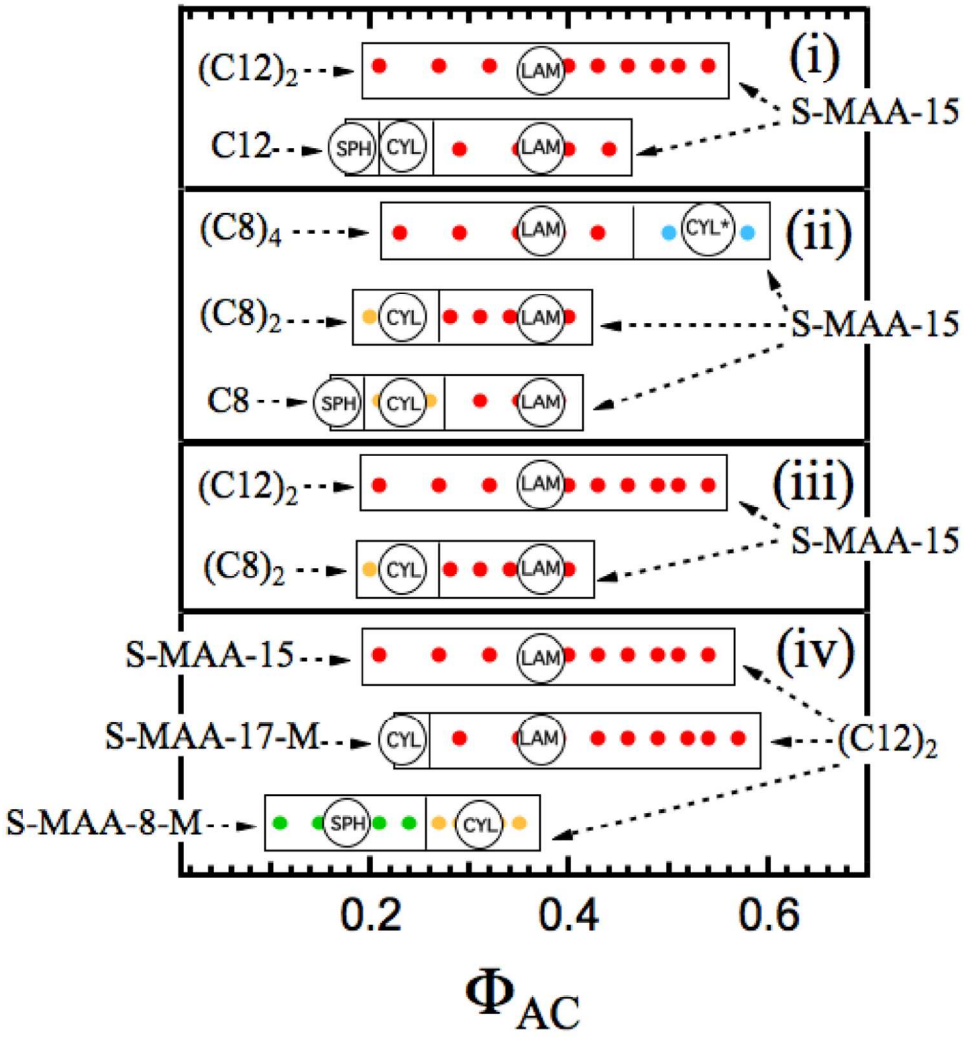

Figure 3. Microdomain morphology diagrams of various L-*b*-AC ionic supramolecules are shown as a function of the volume fraction of the AC-block Φ_{AC} when [(i) and (ii)] the number of alkyl chains (tails) at a side-chain branch point (*m*), (iii) the length of the alky side-chain (l_{sc}), or (iv) the parent diblock copolymer is changed. In (i)-(iv), whenever the parent diblock copolymer or the side-chain type is changed, it is mentioned on the left, and whenever it is unchanged, it is mentioned on the right side of the morphology diagram. (AC-block)-filled spherical microdomains in liquid-like state or body-centered-cubic arrangement (the latter only observed for the data taken from ref. 12) (SPH) [green], (AC-block)-filled hexagonally-packed cylindrical (CYL) [yellow], alternating lamellar microlayers of AC- and L-blocks (LAM) [red], and (L-block)-filled hexagonally-packed cylindrical (CYL*) [blue] microdomain morphologies are indicated. Data of systems of S-MAA-15/C12/X and S-MAA-15/C8/X are taken from ref.[12]

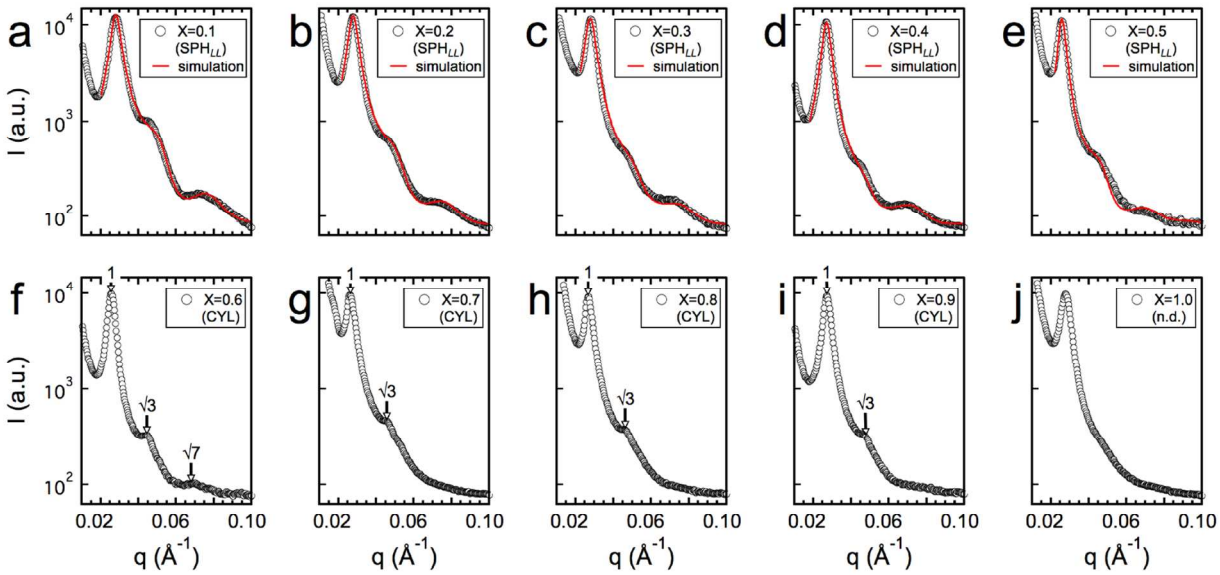

Figure 4. SAXS patterns of L-*b*-AC ionic supramolecules of S-MAA-8-M/$(C12)_2$/X are shown for (a) X=0.1, (b) X=0.2, (c) X=0.3, (d) X=0.4, (e) X=0.5, (f) X=0.6, (g) X=0.7, (h) X=0.8, (i) X=0.9, and (j) X=1.0. In (f)-(i), the observed reflections of the CYL microdomain morphology are indicated. In (a)-(e), the red lines are the simulated intensities of the proposed model of SPH$_{LL}$ microdomain morphology [eqns. (SI-2)-(SI-6) of the Supplementary Information; for details of the simulation, we refer to the Supplementary Information].

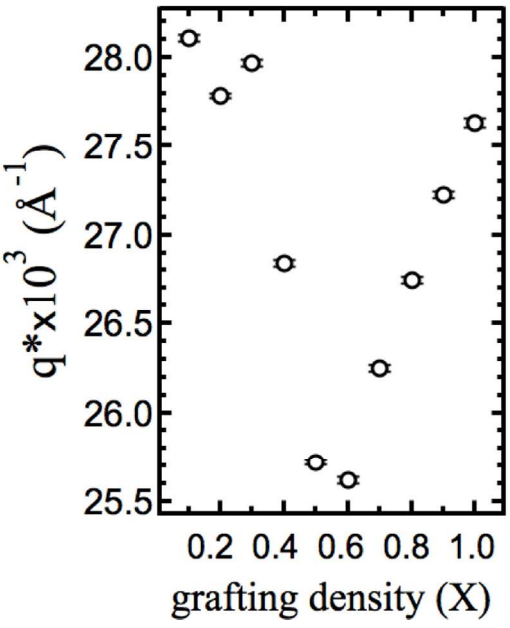

Figure 5. Variation of the position of the first SAXS peak (q^*) of systems of S-MAA-8-M/$(C12)_2$/X ($0.1 \leq X \leq 1.0$) with X is shown. Values of q^* are determined by fitting a Gaussian to the first SAXS peak of the data of Figure 4.

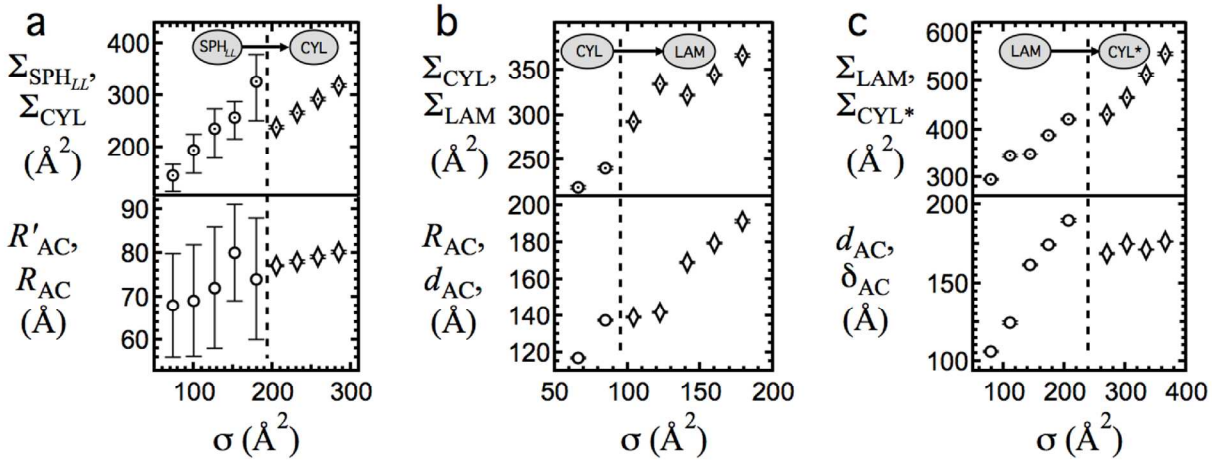

Figure 6. Variations of the interfacial area per block junction (symbols with a dot) and the characteristic size of the (AC-block)-filled domains (hollow symbols) for L-*b*-AC ionic supramolecules of (a) S-MAA-8-M/$(C12)_2$/X [microdomain morphologies of SPH_{LL} (circle) and CYL (diamond)], (b) S-MAA-15/$(C8)_2$/X [microdomain morphologies of CYL (circle) and LAM (diamond)], and (c) S-MAA-15/$(C8)_4$/X [microdomain morphologies of LAM (circle) and CYL* (diamond)] with the average molecular cross-sectional area of an AC-block σ are shown.

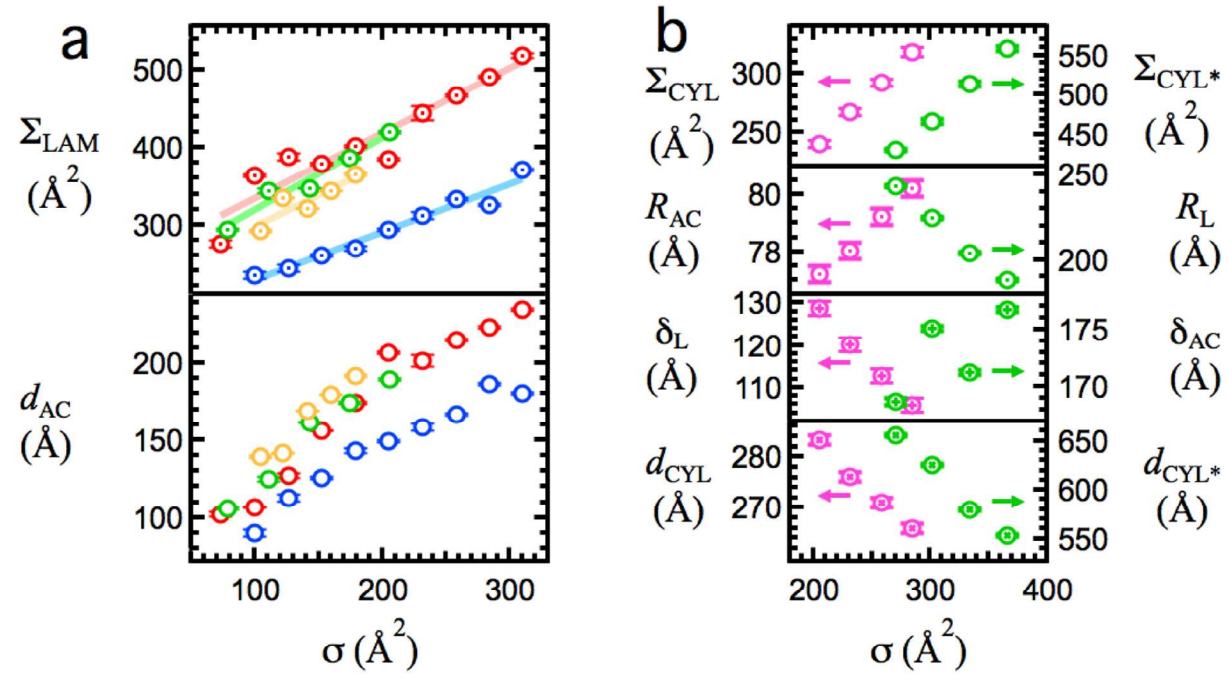

Figure 7. Variations of the size characteristics of L-*b*-AC ionic supramolecules of S-MAA-15/$(C12)_2$/X [red], S-MAA-15/$(C8)_2$/X [yellow], S-MAA-15/$(C8)_4$/X [green], S-MAA-17-M/$(C12)_2$/X [dark blue], and S-MAA-8-M/$(C12)_2$/X [pink] exhibiting microdomain morphologies of (a) LAM [the interfacial area per block junction (circles with a dot) and the thickness of the microlayer of the AC-block (hollow circles)], and/or (b) CYL [the interfacial area per block junction (hollow circles), the radius of the (AC-block)-filled cylinders (circles with a dot), the minimum distance between (AC-block)-filled cylinders (circles with a plus) and the repeat distance of the structure (circles with a cross)] and CYL* [the interfacial area per block junction (hollow circles), the radius of the (L-block)-filled cylinders (circles with a dot), the minimum distance between (L-block)-filled cylinders (circles with a plus) and the repeat distance of the structure (circles with a cross)] with the average molecular cross-sectional area of the AC-block σ are shown. In (a) the solid lines are the results of line-fittings to the data.

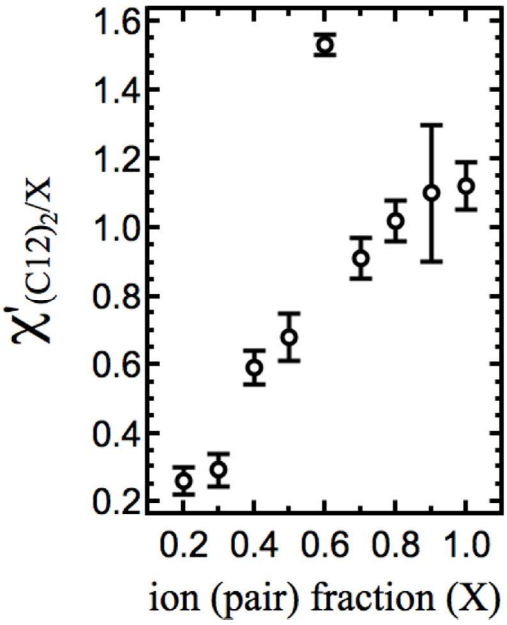

Figure 8. For $(C12)_2$-type counter-ion neutralized L-*b*-AC ionic supramolecules, the determined effective Flory-Huggins interaction parameter between L- and AC-blocks [$\chi'_{(C12)_2/X}$] is shown as a function of the ion (pair) fraction (X).

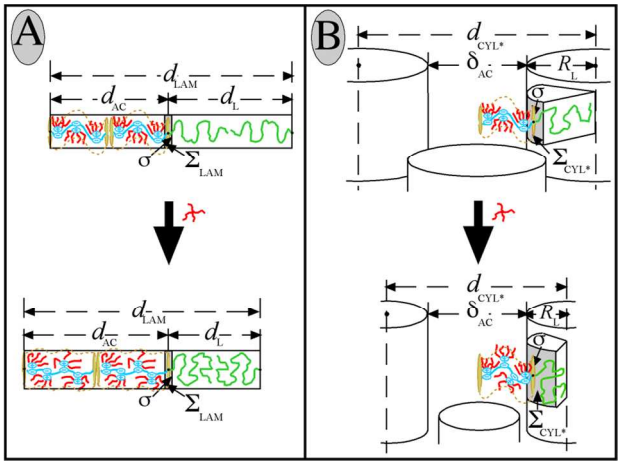

Scheme 2. Schematics of the effects of increasing the side-chain grafting density X of a L-*b*-AC ionic supramolecule of S-MAA-15/$(C8)_4$/X on the size characteristics of its (A) LAM microdomain morphology (occurring for samples with X-values in the range of $0.1 \leq X \leq 0.5$), and (B) CYL* microdomain morphology (occurring for samples with X-values in the range of $0.7 \leq X \leq 1.0$).

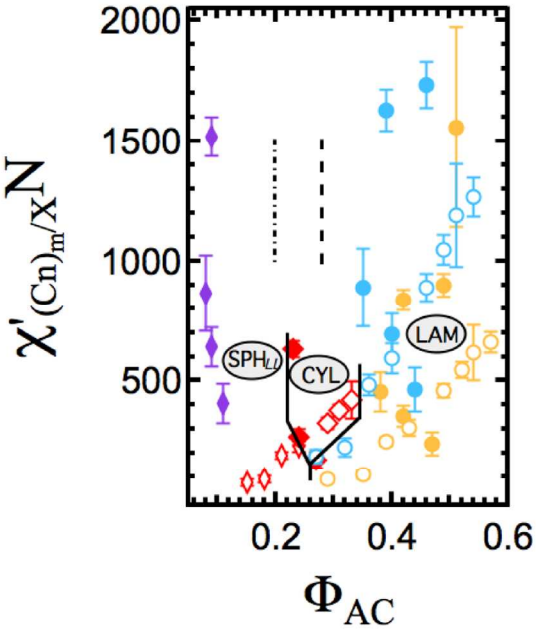

Figure 9. Microdomain morphology diagram of single-tail (filled symbols; data taken from refs.[12, 23]) and multi-tail (hollow symbols; data of the present paper) L-*b*-AC ionic supramolecules for which the value of the effective Flory-Huggins interaction parameter between L- and AC-blocks [$\chi'_{(Cn)_m/X}$] is known, is presented in the format of the effective degree of micro-segregation between L- and AC-blocks [$\chi'_{(Cn)_m/X}N$] *vs.* the volume fraction of the AC-block (Φ_{AC}). The parent diblock copolymers of these systems are S-MAA-3 (purple; S-MAA-3 has a total molecular weight of $\cong 48$ kg/mol and a composition of $\Phi_{PMAA} \cong 0.03$ [ref.[31]]), S-MAA-8-M (red), S-MAA-15 (blue), and S-MAA-17-M (yellow). The microdomain morphologies are SPH$_{LL}$ (narrow diamonds), CYL (wide diamonds), and LAM (circles). From ref.[12], for single-tail containing L-*b*-AC ionic supramolecules, the morphological boundaries of SPH$_{LL}$/CYL (dashed-dotted line) and CYL/LAM (dashed line) are reproduced. The solid lines separate areas occupied by various microdomain morphologies.

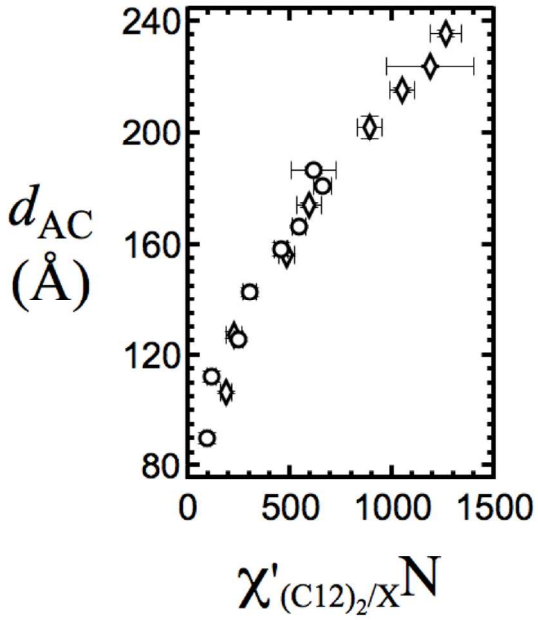

Figure 10. Variation of the thickness of the microlayer of AC-block (d_{AC}) with the effective degree of micro-segregation [$\chi'_{(C12)_2/X}N$] is shown for $(C12)_2$ containing L-*b*-AC ionic supramolecules that are based on parent diblock copolymers of S-MAA-15 (diamond) and S-MAA-17-M (circle).

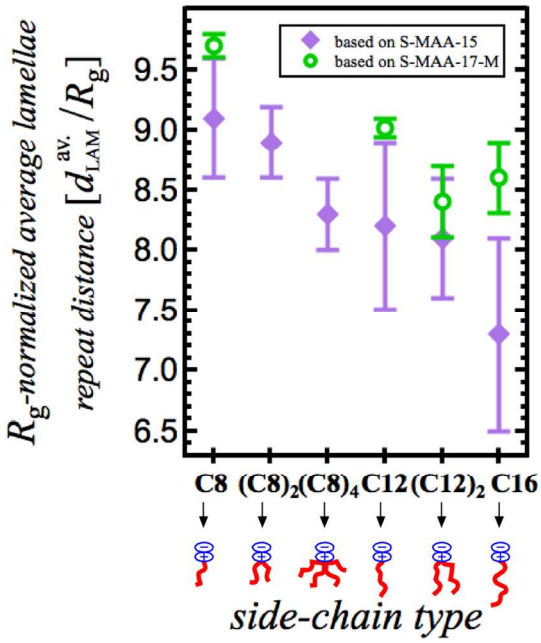

Figure 11. For lamellae-forming L-*b*-AC ionic supramolecules based on parent diblock copolymers of S-MAA-15 (purple filled diamonds) and S-MAA-17-M (green hollow circles), the parameter $d_{LAM}^{av.}/R_g$ is shown for systems with different side-chain types. For each data point, the error bars correspond to the standard deviation. For C8-, C12-, and C16-containing systems, the data are taken from refs.[12, 23]